Peptide−TiO_2 Surface Interaction in Solution by Ab Initio and Molecular Dynamics Simulations

Vincenzo Carravetta* and Susanna Monti

Istituto per i Processi Chimico-Fisici, Area della Ricerca, via G. Moruzzi 1, I-56124 Pisa, Italy

Received: November 22, 2005; In Final Form: January 25, 2006

Ab initio periodic calculations and classical molecular dynamics (MD) simulations were performed to investigate the adsorption mode of alanine and a number of short peptides, in particular two peptides, alanine−glutamic acid and alanine−lysine, taken as model systems for the ionic self-complementary oligopeptide EAK16-II, onto TiO_2 (110) rutile surface, and their conformational characteristics upon adsorption. The atomistic description of the rutile surface and its interactions with water and peptide molecules were based on ab initio calculations, the TIP3P water model, the AMBER force field, and available parameters. By comparison with ab initio calculations, it is shown that MD simulations of reasonable duration can describe the main characteristics of the peptide−TiO_2 surface interaction in solution, at least on a short time scale. Atom−atom radial distribution functions, atom−surface distances, backbone and side chain dihedral angle distributions, and peptide−surface interaction energies have been analyzed. Once adsorbed onto the TiO_2 rutile surface by a bidentate interaction of both carboxyl oxygens with two adiacent Ti atoms, the small peptide studied showed a clear propensity to remain there and undergo relatively limited hinge-bending motions.

1. Introduction

A very interesting and new class of biomaterials is represented by ionic self-complementary oligopeptides,[1] short and extremely versatile peptide molecules easy to design and synthesize, containing hydrophobic and hydrophilic residues assembled in regularly organized sequences. Biocompatibility and biodegradability make this class of compounds most suitable in a number of applications in both the biomedical and the pharmaceutical sectors. Self-complementary oligopeptides are used as matrixes in tissue engineering and carriers in drug delivery systems.[1−10] They play an active role in cell adhesion, cell morphologies, and cell functions; their matrixes support mammalian cell attachment and do not induce any measurable immune response or tissue inflammation when introduced into animals.[3]

EAK16-II is a typical member of this self-assembly oligopeptide family, and it is formed by the hydrophobic alanine (Ala) and hydrophilic glutamic acid (Glu) and lysine (Lys) residues (16 amino acids in all), arranged in an alternating two negative and two positive charge sequence (− − + + − − + +).[4] The spontaneous self-aggregation mechanism of EAK16-II molecules, conformations, and the appearance of macroscopic structures have been extensively studied through different experimental techniques,[11−14] whereas theoretical investigations have made only slow progress due to the difficulty to correctly describe and take into account the various intra- and intermolecular interactions that play a crucial role in the formation of the supramolecular structures. Recently, Chen et al.[15] have shown, using a combination of experimental and theoretical methods, that single-molecule properties have a critical influence on the self-assembly of charged oligopeptides. Their coarse-grained charged wormlike chain model was revealed to be useful in studying the competition between intrachain electrostatic interactions and the bending energy of EAK16-II molecules.

In the present study, starting from the minimum energy conformations obtained through Metropolis Monte Carlo simulations by Chen et al. and kindly made available to us, atomistic molecular dynamics (MD) simulations have been employed to access information regarding molecular structure and dynamics of two dipeptides (Ala-Glu and Ala-Lys), representing the two extremities of EAK16-II, when interacting with a TiO_2 surface in water solution. It is well-known that titanium dioxide has a great variety of applications in several different areas such as heterogeneous catalysis and photocatalysis, sensoristics, cosmetics, coating, etc. Ti lightness, excellent mechanical properties, lack of toxicity, and extremely low corrosion rate result in good biocompatibility, a unique characteristic responsible for its successful use as a medical implant and prosthesis material.[16] It is thus interesting to study the interaction mechanisms that take place during the adsorption process of organic macromolecules onto TiO_2 surfaces with the aim of providing a better understanding of the properties of functionalized organic layers. Peptide-based biomaterials can be fabricated by adsorption on TiO_2 surfaces to give rise to self-organized two- and three-dimensional structures (scaffolds), which support three-dimensional tissue growth. Some of the most promising new synthetic biomaterial scaffolds are composed of self-assembling peptides, such as EAK16-II, that can be modified to contain biologically active motifs.[17] The development of synthetic materials promoting cell growth aims at the realization of systems suitable for implantology or sensoristic applications. Self-assembling peptides have already been employed as substrates for neurite growth and synapsis formation[3,18] and as scaffolds for cartilage tissue repair.[19]

Since EAK16-II peptides are composed of Ala, Lys, and Glu amino acids, examination of the adsorption properties of model Ala-Lys and Ala-Glu dipeptides may provide useful information about the EAK16-II−surface interactions that are obscured in a more complex model macrostructure. From this point of view, the present paper should be considered a first report on a more

* Author to whom correspondence should be addressed. Phone: +39-050-3152521. Fax: +39-050-3152230. E-mail: v.carravetta@ipcf.cnr.it.

10.1021/jp056760j CCC: $33.50
Published on Web 03/03/2006

extended study that aims at investigating different adsorption mechanisms on TiO_2 for the two model dipeptides and finally for the EAK16-II peptide itself.

The extension of the model needed to adequately simulate the system under investigation, in terms of size of the adsorbate and of the portion of surface involved as well as of number of water molecules to be included for describing solvent effects, suggests adoption of a molecular dynamics approach. The main advantage of MD, largely and successfully applied to the simulation of biochemical systems, is in the reasonable computational cost in the simulation of complex systems where different interaction mechanisms cannot be practically treated at a more sophisticated ab initio level. However, to obtain a clearer and more complete picture of the system, our MD simulations were complemented by other computational techniques, namely, ab initio Møller−Plesset second-order perturbation theory (MP2) and periodic density functional theory (DFT) calculations.

The computational procedure adopted consisted of several steps:

- ab initio determination of force field parameters needed for the MD calculation and not available in the literature;
- periodic DFT calculations to estimate the strength of two possible and distinct binding modes of a single amino acid (Ala) on the TiO_2 rutile surface (110);
- MD simulations of the Ala adsorption process onto TiO_2 (110) in water solution (binding mode evaluation);
- MD simulations of adsorption of two dipeptide segments.

In section 2 the main characteristics of the physical and computational model adopted are briefly described. The results of the simulations for the adsorption of Ala, with different terminations, namely, acetyl (Ala-Ace) and *N*-methylamine (Ala-Nme) groups, are reported in section 3. The simulation data regarding Ala-Glu and Ala-Lys adsorption onto the TiO_2 rutile surface are presented and discussed in section 4.

2. Physical and Computational Model

The interaction mechanisms that take place during the adsorption of a large organic molecule on a surface are complex and depend on several characteristics of the full system, including the nature of the adsorbed species, the structure of the surface, the presence of a solvent, etc. To perform a well-defined investigation of the processes involved in the adsorption of peptides on titanium oxide, we had to focus on a well-defined system. This was done starting from the choice of a specific surface of TiO_2, rutile (110), on which the deposition is supposed to occur from an aqueous solution of the peptide.

2.1. Titanium Dioxide Surface. The TiO_2 rutile (110) surface, which is the most stable crystal face, is characterized by a plane of Ti atoms including rows of exposed, fivefold Ti sites and rows of doubly coordinated bridging O atoms that protrude above the surface and are bound to two sixfold Ti atoms located in the surface plane. Rows of exposed threefold oxygens are also included in the surface plane. In the present context of interaction of the surface with an aqueous solution of peptides, each exposed terminal Ti site can be considered to be covered by a strongly associated water molecule.

The nonhydroxylated (110) surface (Figure 1) stems from the relaxation of the rutile bulk structure cleaved by the (110) plane. It is known that every surface relaxes to some extent, but from symmetry considerations, the main relaxations occur perpendicular to the surface. According to X-ray crystal truncation rod studies of a rutile (110) single crystal, the relaxation of the surface in contact with an aqueous solution at room temperature is minimal.[20] Theoretical studies by other authors[21] confirmed, in agreement with the experimental data, that the motions of the surface atoms were quite limited and did not affect the simulation results.

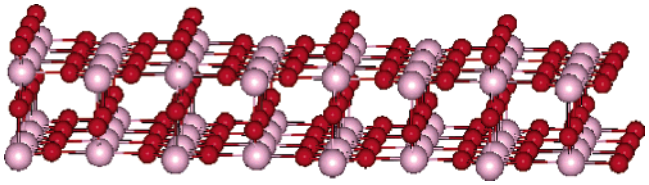

Figure 1. Ball-and-stick model of two planes of a portion of the perfect TiO_2 rutile (110) surface used in DFT calculations and MD simulations. Pink balls represent Ti atoms whereas red balls represent oxygen atoms.

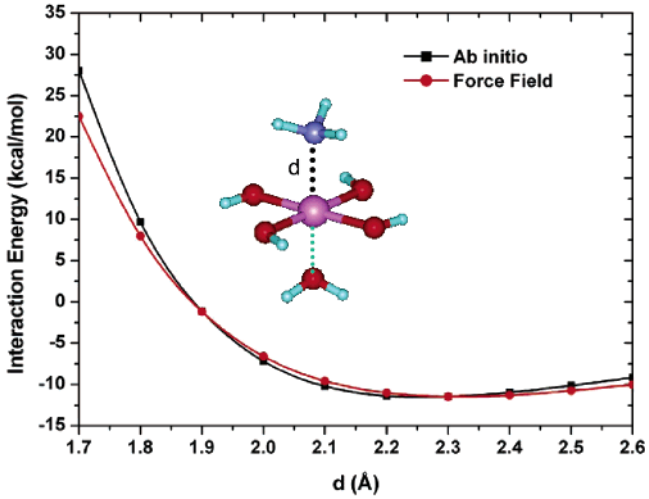

Figure 2. Rigid model consisting of an NH_3 molecule complexed with a TiO_5H_6 cluster. A comparison between the MP2 BSSE-corrected binding energy and the parametrized force field is shown.

The rutile surface structure was created using Cerius[2] software[22] by periodic replication, in both *x*- and *y*-directions where periodic boundary conditions were used, of an elementary cell containing four surface Ti atoms, four surface oxygen atoms, and two bridging oxygens leading, to a MD simulation box whose *xy*-size was 52×27 Å^2.

2.2. Force Field Parameters. The interaction potential parameters necessary to carry out molecular dynamics simulations of the rutile/oligopeptide/aqueous solution system were taken from published data,[23,24] existing force fields,[25] and parameters derived, when missing, using a procedure similar to that reported in ref 23. Water molecules were described using the TIP3P model,[26] and the AMBER Cornell et al. force field[25] was employed to adequately represent peptide structures.

To derive the force field parameters, for realistic representation of the peptide structural and dynamic properties in proximity to the TiO_2 surface, ab initio calculations were performed using representative model systems. Extensive quantum mechanical calculations are, in fact, prohibitively expensive for a detailed description of the system under study; thus rigid models consisting of small molecules (H_2CO and NH_3) complexed with a TiO_5H_6 cluster were employed (Figure 2). The geometry of the TiO_5H_6 cluster was frozen to that of the rutile crystal surface, and binding energies to the different model molecules, defined as the energy of the complex minus the energies of the isolated partners, were calculated using the MP2 method with a mixed basis set: 6-311+G** for Ti atoms and aug-cc-pVDZ for O, C, N, and H atoms, as implemented in Gaussian 03.[27] The binding energies were also corrected for the basis set superposition error (BSSE) using the counterpoise (CP) method.[28,29] The

force field parameters were then derived upon the basis of the complex energetics, choosing a force field form like the one reported in ref 23, and were used in subsequent molecular dynamics simulations. Van der Waals force field parameters can be found in the Supporting Information.

Water is one of the most important adsorbates at the TiO_2 surface. Its interaction with it, which has been investigated in recent years with a variety of experimental and theoretical techniques, can easily affect adsorption and reaction processes of other molecules on the surface. Results from different spectroscopies generally indicate that water adsorbs both dissociatively and molecularly on a perfect TiO_2 rutile (110) surface.[30] However, there is a considerable disagreement on the initial adsorption behavior of water, especially between theoretical and experimental studies. While most of the experimental results agree that water does not dissociate on TiO_2 (110), except at defect sites, some theoretical studies predict dissociative adsorption while other ones do not predict dissociation.[31,32] The TIP3P model, as most of the water models used in simulations, does not allow for dissociation of water molecules; thus this particular aspect has not been taken into account, but the TIP3P model adequately describes water structural and thermodynamical properties.

2.3. Molecular Dynamics Simulation Protocol. To simulate realistically the deposition of peptides from an aqueous solution, the adsorbates made of the TiO_2 rutile (110) surface, comprising two layers formed by 256 Ti and 512 O atoms, and the peptide molecule were solvated creating around them a $52 \times 27 \times 52$ $Å^3$ box containing 904 water molecules. Periodic boundary conditions were applied in the two directions defining the surface. The simulations were carried out with the DLPOLY package.[33] All of the simulations were performed at $T = 310$ K in the NVT ensemble using the Nosé−Hoover thermostat[34] with a relaxation constant of 0.5 ps, and the equations of motion were solved with the Verlet leapfrog algorithm[35] using a time step of 0.001 ps. The SHAKE algorithm[36] was used to constrain all bond lengths of the peptide molecules. The surface geometry was frozen during the whole simulation time. The cutoff for the van der Waals interactions was set to 12 Å, and electrostatic interactions were handled by the reaction field method using the permittivity constant $\epsilon = 78.5$. The validity of the reaction field method was checked by performing one MD simulation with a standard Coulombic potential. No significant structural or dynamical differences were found between both techniques; thus the reaction field approach was used for all of the simulations. The systems were initially minimized to remove bad steric contacts at the box boundaries and then relaxed at constant temperature and volume over 20 ps of dynamics, freezing the solute coordinates to randomize the positions of the solvent molecules; then the constraints were removed, and the systems were equilibrated for 30 ps with 25 kcal mol^{-1} $Å^{-2}$ position restraints on the peptide carboxyl oxygen atoms in contact with the surface to prepare the systems in a form such that unphysical forces did not cause improbable displacements. The resulting configurations were then equilibrated without any constraint for 150 ps.

Starting from the last equilibrium configurations obtained, production runs in the NVT ensemble with total simulation times between 500 and 2500 ps were performed for structural and energetic data collection.

2.4. Periodic Density Functional Theory Calculations. Density functional theory calculations for studying the adsorption of small organic molecules on different surfaces have already been successfully employed.[37−40] They are, presently, computationally prohibitive for studying oligopeptides; however we adopted them for investigating the adsorption of a single amino acid (Ala) on TiO_2 to validate the MD approach applied to the simulation of larger systems.

In principle amino acids may interact with the dehydroxylated TiO_2 surface through different groups,[41] but it has been observed experimentally that in acidic solutions, where Glu and Lys side chains as well as the peptide terminal groups are charged, the binding involves principally the carboxylate groups and Ti atoms.[16] The coordination may be either monodentate or bidentate depending on the number of oxygens used by the molecule to coordinate the surface sites, but the bidentate configuration is strongly favored especially on rutile (110) surface where it can be well accommodated in the channels formed by the rows of the twofold coordinated oxygens.[37,42,43]

This was verified using a plane wave total energy code (DACAPO[44,45]) to optimize a model system made of a two-layer slab of TiO_2 (110) periodically repeated. In the direction that was perpendicular to the metal oxide surface plane, a vacuum of 30 Å was used to separate the slabs. All of the surface atoms were fixed at the crystal geometry. The core electrons of all of the atoms were treated via the ultrasoft pseudopotentials with an energy cutoff of 340 eV for both the electronic wave function and the density. The PW91 gradient-corrected exchange−correlation functional was used in the self-consistent DFT calculations.

Two binding possibilities for the adsorption of an Ala molecule onto the Ti rutile (110) surface were considered in the present study; they have been chosen as corresponding to the most probable adsorption mechanisms according to chemical intuition. Other binding geometries are, in principle, possible, and their relevance will be the subject of further investigations. In the first starting geometry, monodentate adsorption, one of the Ala carboxyl oxygens was aligned vertically with a Ti atom in such a way that the $\angle Ti-O-C_{COO^-}$ angle was equal to 180° and the initial Ti ···O distance was set to 1.8 Å. After energy optimization no substantial rearrangement of the adsorbed species occurred, but just a lengthening of the Ti···O distance from 1.8 to 1.93 Å was observed. The single contact point was maintained.

In the second starting conformation, bidentate adsorption, both carboxyl oxygens were coordinated to two adjacent Ti atoms and placed vertically at initial Ti···O distances of 1.8 Å. The most significant modification after optimization was, also in this case, a lengthening of the Ti···O distances from 1.8 to 2.02 Å and to 1.98 Å, respectively. The binding energy of the monodentate adsorption geometry was largely unfavored (about −0.8 eV) with respect to the bidentate one. This is in agreement with previous theoretical and experimental investigations on bi-isonicotinic acid,[42,43] which proposed an adsorption structure, derived from the calculations and consistent with the experimental data, where the molecule bound to two neighboring Ti rows in a bidentate fashion through the dehydroxylated oxygen atoms. We present in Figure 3 the optimized geometry of the Ala−TiO_2 adsorbate as obtained by the present DFT calculation.

3. Molecular Dynamics Simulations of Alanine Adsorption

Taking into account the experimental and theoretical observations, to test if the C-termini could be directly adsorbed onto the surface, an Ala residue (which does not possess a reactive side chain) terminated with a carboxyl group and with a $-COCH_3$ group to have a peptide bond on account of the continuation of the peptide sequence, was considered (Figure 4). This fragment, hereafter called Ala-Ace, whose total charge

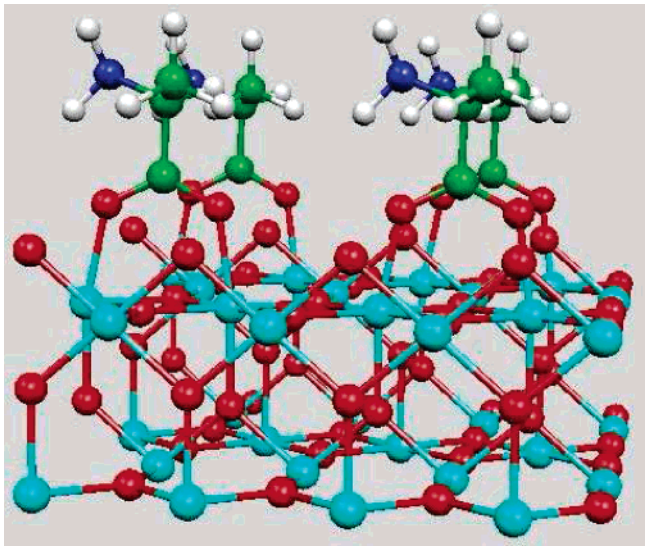

Figure 3. Optimized geometry of alanine adsorbed on a two-layered (110) slab of TiO_2 rutile. The unit cell of 8 Ti atoms, 14 O atoms, and 1 alanine molecule is repeated four times

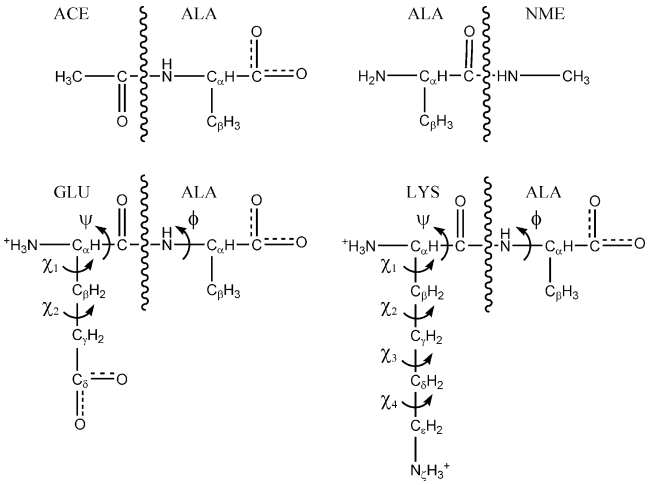

Figure 4. Schematic representation of the peptide segments studied by molecular dynamics simulations.

was equal to −1, was placed near the surface with the two carboxyl oxygens at an initial distance of 1.8 Å from two adjacent Ti central sites, and the molecular dynamics equilibration protocol was applied. Starting from the last equilibrium configuration obtained, a production run 500 ps long was performed. The distribution of water molecules over the surface and around the peptide carbonyl and carboxyl oxygens and the amide hydrogen were quantified by radial distribution functions (RDFs). To be able to better understand the influence of the various chemical groups on adsorption geometry and to predict the existence of possible types of adsorption sites together with their location, atom−atom distances and atom−surface distance variations during the whole simulation time were investigated. The peptide−surface interaction energy was also analyzed.

3.1. Radial Distribution Functions. Ti···water oxygen (OW) and surface oxygen (O_{surf})···water hydrogen (HW) RDFs are shown in Figure S1 in the Supporting Information; peptide carboxyl oxygens (O_{COO^-})···HW, peptide carbonyl oxygen (O_{CO})···HW, and peptide amide hydrogen (H_{NH})···OW RDFs of Ala-Ace are shown in Figure 5. Ti···OW has a sharp first neighbor peak centered at ∼2.0 Å that corresponds to the first layer of molecularly adsorbed water molecules, whereas the well separated lower and broader second peak centered at ∼3.8 Å

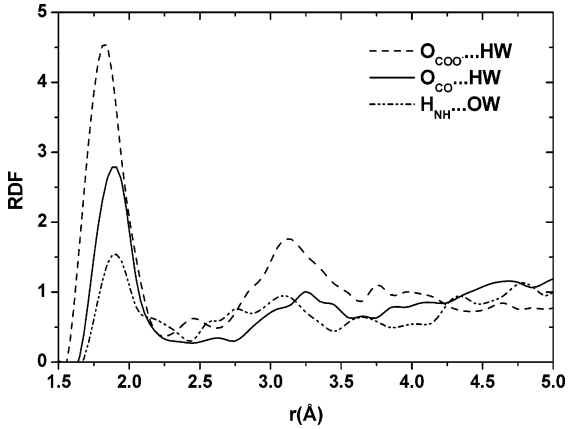

Figure 5. Ala-Ace carboxyl oxygens (O_{COO^-})···HW, Ala-Ace carbonyl oxygen (O_{CO})···HW, and Ala-Ace amide hydrogen (H_{NH})···OW RDFs.

corresponds to the second solvation layer, that is water molecules interacting with the first layer of the terminal and bridging oxygens.

The data are in excellent agreement with X-ray experimental findingsm[20] which give average positions of 2.1 and 3.8 Å for the first and second peak, respectively. The coverage of the first layer in the range 1.8−2.3 Å is exactly one water molecule per terminal Ti, which corresponds to a totally hydrated surface. The presence of a very low amplitude of RDF between the first and the second peak indicates that water molecules do not diffuse but are truly adsorbed onto the TiO_2 surface.

The O_{surf}···HW radial distribution function (Figure S1 in the Supporting Information) shows a first peak for the first solvation shell with a maximum at a distance of 1.9 Å and a second shoulder at about 3.1 Å. During the whole simulation time, water molecules approach surface oxygen atoms at a hydrogen-bonding distance and, in contrast to the waters adsorbed onto Ti atoms, exchange extensively between the first and the second solvation shells, as is confirmed by the presence of an appreciable RDF amplitude between the two regions.

The O_{COO^-}···HW and O_{CO}···HW RDFs (Figure 5) are quite similar to each other, exhibiting a first sharp peak at ideal hydrogen bond distances of about 1.8 and 1.9 Å with coordination numbers of 2.9 and 2.4, respectively. A second broader and lower peak centered at about 3.2 Å is also observed.

The H_{NH}···OW RDF (Figure 5) first distinct peak appears at 1.9 Å with a coordination number of 0.7, which also in this case gives indication of a hydrogen-bond-like arrangement but with a lower number of coordinated water molecules with respect to the Ala oxygens. The second coordination shell of H_{NH} is represented, instead, by a diffuse peak centered at about 2.8 Å.

3.2. Atom−Atom and Atom−Surface Distances. A detailed analysis of the atomic mobilities, expressed in terms of atom−surface distances of Ala-Ace carboxyl oxygens, carbonyl oxygen, and amide hydrogen, is displayed in Figure 6, and the corresponding statistical parameters are reported in Table 1. As it can be seen clearly, both carboxyl oxygens, which are in close contact with two adjacent Ti surface atoms, are restricted in their movement and substantially remain at a distance of about 2.16 Å from the titanium sites during the time scale sampled. Indeed, the Ti···O_{COO^-} distances oscillate between 1.99 and 2.45 Å with standard deviations σ of about 0.1 Å, and the O_{COO^-}−surface distances fluctuate between 1.87 and 2.29 Å with similar σ values.

The curves corresponding to O_{CO} and H_{NH} surface distances have instead more marked fluctuations due to the decreased

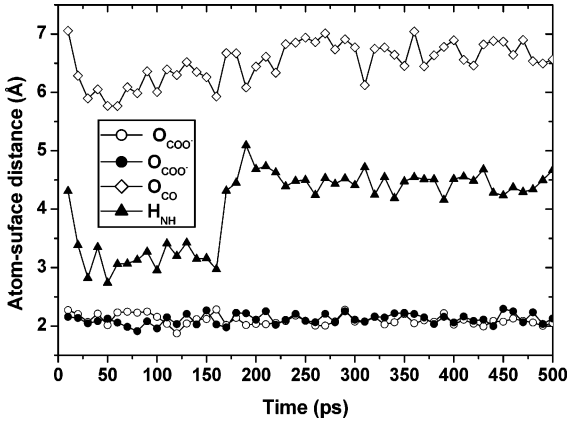

Figure 6. Evolution of the Ala-Ace atom−surface distances during the molecular dynamics simulation time.

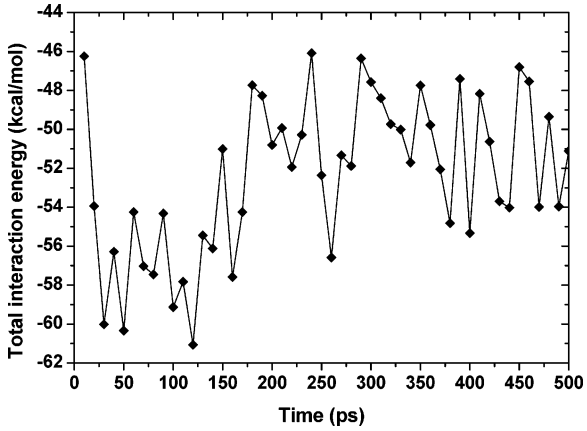

Figure 7. Evolution of the Ala-Ace−surface interaction energy during the molecular dynamics simulation time.

TABLE 1: Statistical Analysis of Atom−Surface Distances (Å)

atom	max	min	mean	σ
		Ala-Ace		
O_{COO^-}	2.29	1.91	2.12	0.09
O_{COO^-}	2.28	1.87	2.10	0.09
O_{CO}	7.05	5.77	6.52	0.35
H_{NH}	5.09	2.74	4.07	0.65
		Ala-Nme		
O_{CO}	2.40	1.99	2.10	0.08
H_{NH_2}	2.42	2.04	2.20	0.08

influence of the surface atoms and to the significantly increased interaction with the surrounding water molecules. However, the O_{CO} fluctuation range (1.28 Å) is smaller than the H_{NH} one (2.35 Å). As it can be observed in Figure 6, H_{NH} reaches the surface at a hydrogen-bonding distance within the first 30 ps of the simulation time, remains almost stable for 130 ps, and then increases its separation toward the final value of about 4.5 Å. A similar, but less remarkable, trend is observed for the carbonyl group. This behavior might be due to the orientation assumed by the NH group after equilibration, to its nearness to the carboxyl moiety, and to the conserved binding position of the carboxyl oxygens in the adsorbate at equilibrium.

3.3. Ala-Ace−Surface Interaction Energy. The interaction energy between Ala-Ace and the (110) TiO_2 rutile surface as a function of time is shown in Figure 7. Such energy fluctuates around −52.4 kcal/mol (σ = 4.0 kcal/mol), exploring a range of about 15 kcal/mol. A shift toward more negative values (i.e., more favorable interactions between the peptide and the TiO_2 surface) occurs around 30 ps, and exactly at the same time a jump in the H_{NH} surface distance plot toward shorter atom−surface separations is observed (Figure 6). These stronger interactions are maintained for about 130 ps, then at around 160 ps another shift, but this time toward less negative values (i.e., more unfavorable interactions) and a corresponding increase of the H_{NH} surface distance, is noticed. These results suggest that, notwithstanding the presence of the screening water molecules, the peptide can reorientate itself in such a way to maximize the number of favorable contacts, which can be water-mediated, with the surface atoms while preserving the bidentate attachment.

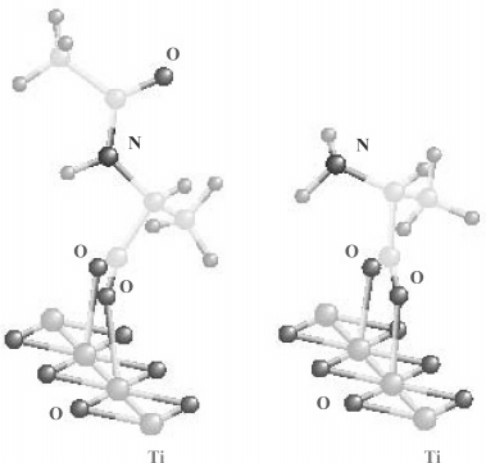

Figure 8. Comparison of an MD-extracted structure of the Ala-Ace + (110) TiO_2 rutile layer + water complex (left) with the DFT-optimized bidentate adsorbed conformation of Ala (right). Only a small portion of the TiO_2 surface is visible, and water molecules have been omitted for clarity. Carbon atoms are in light gray.

The comparison of the molecular dynamics results with experimental data found in the literature and with the periodic DFT-optimized Ala adsorption structure, discussed in the previous section (Figure 8), shows that the parameters and the simulation protocol used provide a correct description of a possible Ala adsorption process. The Ti···O_{COO^-} mean distances obtained by DFT calculations are about 2.0 Å, whereas MD simulation mean values are slightly longer (2.1 Å) due to the presence of competing water molecules. However, the overall agreement in derived O_{COO^-} positions is satisfactory and further validates the general approach proposed for the simulation of the adsorption of large peptides on TiO_2 surfaces.

3.4. Binding Mode Evaluation. To test a different binding possibility a neutral Ala residue terminated, this time, with an NH_2 amine group and with an $-NHCH_3$ group, to mimic a peptide bond, hereafter called Ala-Nme, was placed near the surface, orienting the NH_2 nitrogen atom toward a Ti atom, as a starting point for a MD simulation. It was confirmed in several experiments[46−50] as well as theoretical calculations[51,52] that ammonia adsorbs molecularly on TiO_2 (110) surfaces at room temperature, binding with its N end down to the fivefold coordinated Ti atoms.

The Ala-Nme molecule can be considered an appropriate model in a basic environment, while Lys side chains and N-terminal groups are mainly charged at pH < 9. In fact it seems likely that favorable electrostatic interactions are primarily responsible for NH_3^+ amino groups binding to the TiO_2 surface through hydrogen bonds with the oxygen atoms. There is no evidence for positively charged Lys acting as ligands to surface Ti ions. Nevertheless, a neutral amine group could be, in principle, coordinated to the titanium metal center, and we wanted to test this binding possibility.

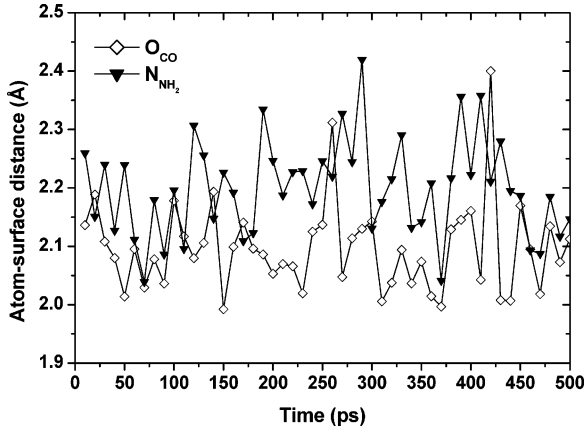

Figure 9. Evolution of the Ala-Nme atom−surface distances during the molecular dynamics simulation time.

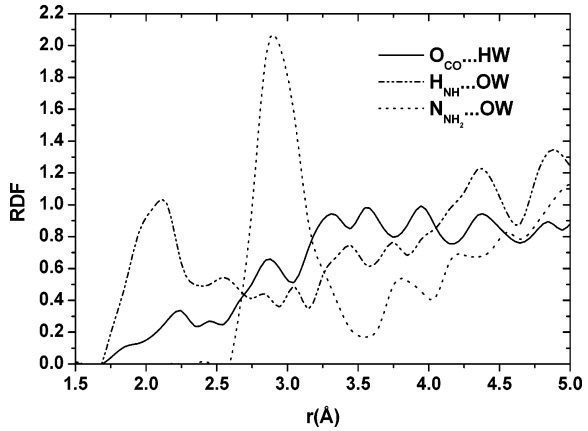

Figure 10. Ala-Nme carbonyl oxygen (O_{CO})···HW, Ala-Nme amide hydrogen (H_{NH})···OW, and Ala-Nme amine nitrogen (N_{NH_2})···OW RDFs.

An almost vertical spatial arrangment of the Ala-Nme molecule, with the NH_2 nitrogen positioned at an initial distance of 1.9 Å from a Ti central site of the surface and the carbonyl oxygen oriented toward the bulk solvent, was chosen as the starting conformation for the MD simulations. During the last steps of the equilibration phase a reorientation of the carbonyl oxygen toward the Ti atom close to the nitrogen bonding titanium, such as to form a heterogeneous bidentate coordination structure, was observed. Furthermore, examination of the Ti···N and Ti···O distance evolution during the production run shows that this binding mode is maintained for the whole simulation time. Indeed, the Ti···N mean distance is about 2.2 Å with a standard deviation of about 0.08 Å while the Ti ···O distance is slightly shorter (2.1 Å and $\sigma = 0.08$ Å). The time evolution of O_{CO} and N_{NH_2} atom surface distances are displayed in Figure 9, and their statistical parameters are reported in Table 1.

The O_{CO}···HW, H_{NH}···OW, and N_{NH_2}···OW RDFs are plotted in Figure 10. A strong difference between the RDF for Ala-Ace O_{CO}···HW (Figure 5) on one hand and the RDF for Ala-Nme O_{CO}···HW (Figure 10) on the other hand can be noticed. The characteristic first peak at short intermolecular distances is missing in the Ala-Nme O_{CO}···HW RDF; instead, a broad shoulder of very low amplitude extending between ∼1.7 and ∼2.4 Å, where the coordination number is about 0.3, is visible, thus confirming that O_{CO}, being engaged in a direct interaction with the surface, is here essentially inactive for hydrogen bonding with water molecules. On the contrary, the regular first maxima at ∼2.1 and ∼2.9 Å and the minima at ∼2.4 and ∼3.6 Å characteristic of hydrogen bonds are present

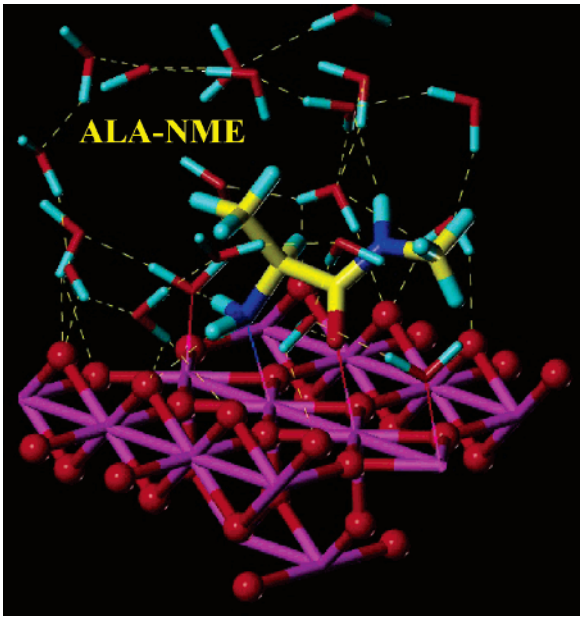

Figure 11. Simulation snapshot showing a representative structure of the Ala-NME + (110) TiO_2 rutile layer + water complex. Only a small portion of the surface and a limited number of water molecules are displayed. Surface atoms are shown in ball-and-stick mode. The green dashed lines show the hydrogen bonds. Color codes: carbon, yellow; hydrogen, cyan; nitrogen, blue; oxygen, red; titanium, magenta.

in the plot of the H_{NH} and N_{NH_2} RDFs, respectively. The coordination numbers derived from the H_{NH}···OW and N_{NH_2}···OW RDFs are 0.7 and 1.7, respectively, suggesting that H_{NH} is involved in one intermolecular hydrogen bond, likewise Ala-Ace H_{NH}, whereas N_{NH_2} could form, if not bound to the Ti site, two simultaneous intermolecular hydrogen bonds with water molecules, on average.

The Ala-Nme−surface interaction energy (Figure S2 in the Supporting Information) oscillates around an average value of −44.0 kcal/mol with a lower deviation ($\sigma = 2.4$ kcal/mol) with respect to the Ala-Ace case. The range of values explored is 4 kcal/mol smaller than the Ala-Ace one, and the values are in general less favorable with respect to the homogeneous bidentate coordination model. The results suggest that the spatial arrangement assumed by the molecule after the equilibration period (Figure 11) limits molecular movements, conformational adjustments, and water accessibility. The tendency of the total interaction energy toward less negative values can be ascribed to the less favorable electrostatic contribution originating from the charge nature of the interacting species.

However, taking into account the environmental conditions and the nature and structure of the interacting species, it can be deduced that heterogeneous bidentate configurations could be present, in principle, but their probability is reduced with respect to homogeneous bidentate adsorption geometries.

4. Molecular Dynamics Simulations of Dipeptide Adsorption

To study some of the interactions responsible for peptide adsorption onto the TiO_2 surface, molecular dynamics simulations were performed on model charged dipeptides: Ala-Glu (having a total charge equal to −1 due to the Glu side chain COO^- group) and Ala-Lys (having a total charge equal to +1 due to the Lys side chain NH_3^+ group); both terminated with COO^- and NH_3^+ groups, extending the total simulation time to 2.5 ns. The longer duration of the simulation should give a more realistic picture of the conformational changes that occur in the dipeptide structures as they relax, interacting with the surround-

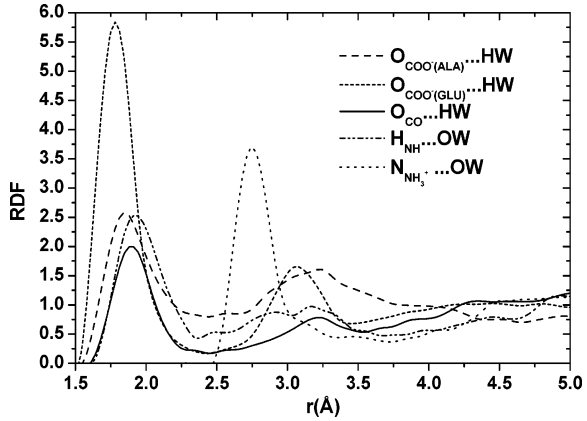

Figure 12. Ala-Glu dipeptide radial distribution functions: Ala carboxyl oxygen ($O_{COO^-(Ala)}$)···HW, Glu carboxyl oxygens ($O_{COO^-(Glu)}$)···HW, carbonyl oxygen (O_{CO})···HW, amide hydrogen (H_{NH})···OW, and amine nitrogen ($N_{NH_3^+-terminus}$)···OW RDFs.

ing environment made of surface atoms and water molecules. The initial conformations, as in the previous cases studied, were extracted from EAK16-II minimum energy structures, and their orientation with respect to the surface was chosen on the basis of Ala-Ac simulation results: a vertical homogeneous bidentate attachment of the C-terminal carboxyl oxygens positioned at an initial distance of 2.1 Å from two titanium adjacent sites.

Atom−atom RDFs, atom−surface distances, backbone and side chain dihedral angle distributions, and peptide−surface interaction energies have been analyzed.

4.1. Dipeptide Ala-Glu: Molecular Dynamics Results. Ala-Glu···water RDFs are plotted in Figure 12. The $O_{COO^-(Ala)}$··· HW RDF shows a peak at 1.85 Å for the first hydration shell and a minimum at ∼2.44 Å, thus yielding a coordination number of about 2.2. Between ∼2.75 and ∼3.55 Å a broad shoulder with a low amplitude can be observed. A similar trend is manifested by both H_{NH}···OW and O_{CO}···HW RDFs but with the first peak centered at 1.92 and 1.90 Å, minima at ∼2.36 and ∼2.30 Å, and coordination numbers of 1.1 and 1.8, respectively. The second shell shoulder is, in both cases, broader and lower than that in the $O_{COO^-(Ala)}$···HW RDF. The $O_{COO^-(Glu)}$···HW RDF, corresponding to the coordinated water sphere around Glu side chain carboxyl oxygens, has a well-defined sharp peak at 1.78 Å, a minimum at about 2.41 Å, and a coordination number of 6.1, indicating that the carbonyl group can be involved in six simultaneous intermolecular hydrogen bonds with water, on average. It is interesting to note the presence of a marked second peak located at 3.07 Å, which can be considered a manifestation of water molecule ordering in a stable second hydration shell around the carboxyl moiety. The $N_{NH_3^+}$···OW RDF exhibits only one sharp peak at about 2.75 Å with a coordination number equal to 3.8.

Ala-Glu atom surface distances are shown in Figure 13, and the corresponding statistical parameters are reported in Table 2. Both terminal Ala carboxyl oxygens remain strongly bonded to the surface titanium atoms for the whole simulation time at an average distance of 2.03 Å, which corresponds to a distance from the surface of about 1.98 Å, and have very small fluctuations around this mean value as confirmed by the standard deviation ($\sigma = 0.5$ Å). Distance fluctuations of the other groups increase with the growth of their separation from the attached portion of the molecule; indeed, Glu carboxyl oxygen distances have larger fluctuations with $\sigma > 1.15$ Å, which, however, do not succeed in shifting this moiety, well-solvated by water, to distances from the surface lower than 5.21 Å throughout 2.5 ns simulation.

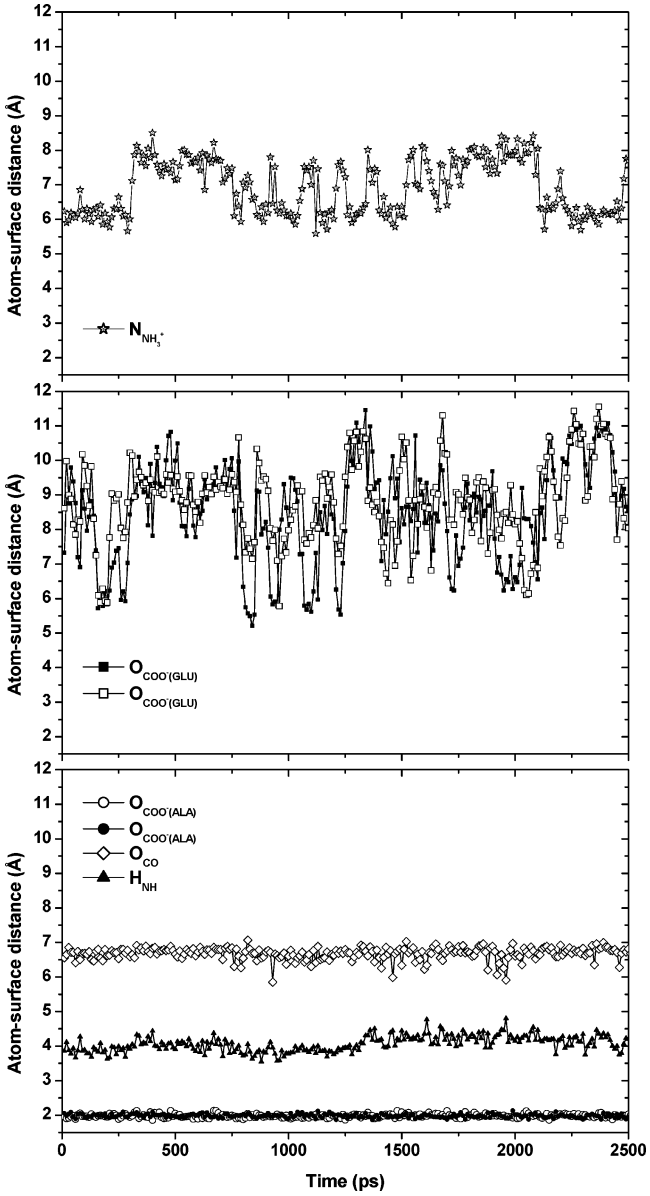

Figure 13. Evolution of the dipeptide Ala-Glu atom−surface distances during the molecular dynamics simulation time.

TABLE 2: Statistical Analysis of Atom−Surface Distances (Å)

atom	max	min	mean	σ
		Ala-Glu		
$O_{COO^-(Ala)}$	2.13	1.86	1.98	0.05
$O_{COO^-(Ala)}$	2.14	1.86	1.98	0.05
$O_{COO^-(Glu)}$	11.45	5.21	8.43	1.44
$O_{COO^-(Glu)}$	11.55	5.78	8.79	1.15
O_{CO}	7.06	5.85	6.68	0.18
H_{NH}	4.80	3.55	4.08	0.11
$N_{NH_3^+-terminus}$	8.50	5.59	6.94	0.78
		Ala-Lys		
O_{COO^-}	2.09	1.84	1.97	0.05
O_{COO^-}	2.15	1.86	2.00	0.05
O_{CO}	6.94	5.98	6.57	0.17
H_{NH}	4.44	3.55	3.86	0.15
$N_{NH_3^+-terminus}$	7.63	5.72	6.34	0.32
$N_{NH_3^+-side\ chain}$	11.33	3.58	6.40	1.31

The total interaction energy is always favorable and fluctuates between −84.7 and −59.4 kcal/mol (Figure S3 in the Supporting Information). The complexes corresponding to more negative interaction energy values are characterized by a network of

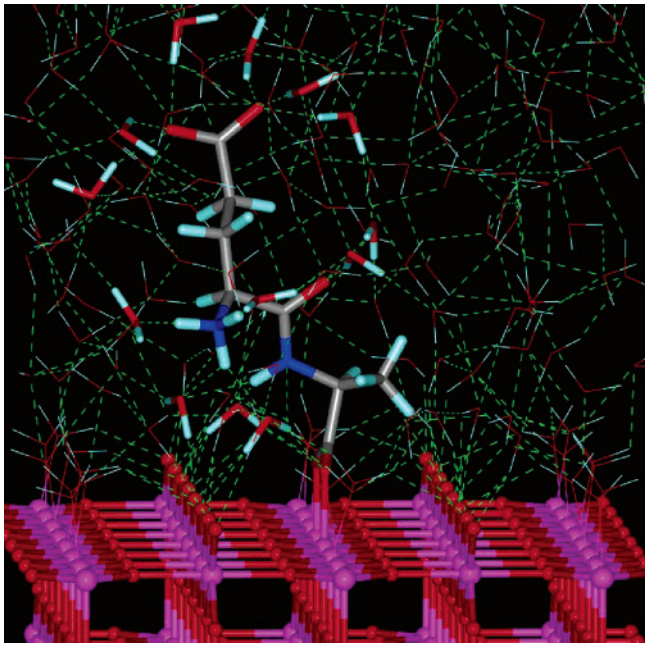

Figure 14. Simulation snapshot showing a representative structure of the Ala-Glu + (110) TiO_2 rutile layer + water complex having more favorable interaction energy values, characterized by a network of hydrogen bonds between the charged N-terminal group and the water molecules adsorbed onto the surface or hydrogen-bonded to the surface oxygen atoms. Only a small portion of the surface and a limited number of water molecules are displayed. Surface atoms are shown in ball-and-stick mode. The green dashed lines show the hydrogen bonds. Water molecules hydrogen-bonded to the peptide hydrophilic groups are shown in stick mode. Color codes: carbon, gray; hydrogen, cyan; nitrogen, blue; oxygen, red; titanium, magenta.

hydrogen bonds between the charged N-terminal group and the water molecules adsorbed onto the surface or hydrogen-bonded to the surface oxygen atoms (Figure 14).

A more detailed description of the conformational dynamics and flexibility of the dipeptide segments can be obtained by analyzing the distribution of backbone and side chain dihedral angles (indicated by arrows in Figure 4) together with their time evolution during the course of the simulation. The distributions of ϕ (C−N−C_α−C) and ψ (N−C_α−C−N) backbone dihedrals are displayed in Figure S4 in the Supporting Information, while the distributions of χ_1 (C−C_α−C_β−C_γ) and χ_2 (C_α−C_β−C_γ−C_δ) side chain dihedrals are shown in Figure S5 in the Supporting Information. The backbone ω dihedral angle (C_α−C−N−C_α), identifying a trans (180°) or cis (0°) arrangement of the peptide bond, oscillates around 180°, implying a trans peptide bond. The ϕ distribution steeply falls from a maximum in the range [−180°,−150°] and vanishes at values beyond −120°. As confirmed by the time evolution plot, ϕ has a small deviation from the starting values as well as small fluctuations. The values assumed by the ψ angle cover, instead, a larger interval between ∼30° and ∼180°; the distributions have a bimodal shape with the first peak at ∼60° and the second peak at ∼120°, and both maxima occur effectively with equal probability. The χ_1 and χ_2 torsion angle distributions exhibit four maxima in the ranges [−180°,−150°], [150°,180°], [−90°,−30°], and [30°,90°] with different probabilities. The results suggest a higher mobility of the side chains with respect to the backbone.

4.2. Dipeptide Ala-Lys: Molecular Dynamics Results. The Ala-Lys···water RDFs are displayed in Figure 15. The $O_{COO^-(Ala)}$···HW and O_{CO}···HW RDFs exhibit a peak for the first solvation shell at a distance of 1.88 Å. Taking the integral

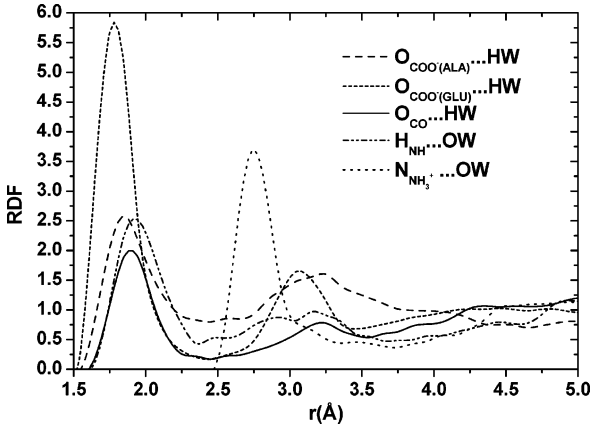

Figure 15. Ala-Lys dipeptide radial distribution functions. Carboxyl oxygens (O_{COO^-})···HW, carbonyl oxygen (O_{CO})···HW, amide hydrogen (H_{NH})···OW, terminus amine nitrogen ($N_{NH_3^+-terminus}$)···OW, and side chain amine nitrogen ($N_{NH_3^+-side\ chain}$)···OW RDFs.

of the curves up to the minimum at ∼2.25 Å for the $O_{COO^-(Ala)}$···HW RDF and at ∼2.59 Å for the O_{CO}···HW RDF, a coordination number of 1.8 is obtained in both cases, indicating that O_{COO^-} and O_{CO} atoms can participate in two hydrogen bonds, on average.

The H_{NH}···OW RDF shows a first peak centered at 1.93 Å, a minimum at 2.27 Å, and a coordination number of 1.0. In contrast with the other cases, a second hydration shell peak, rather weak and diffuse, appears at 3.05 Å, suggesting the existence of a somewhat ordered water structure.

The $N_{NH_3^+}$···OW RDF peak is located at ∼2.77 Å, its minimum is at about 3.6 Å, and there are, on average, 9.6 coordinated water molecules involved in intermolecular interactions with the NH_3^+ groups. A second peak is also visible at 4.8 Å.

Backbone dihedral angle distributions and their time evolutions are displayed in Figure S6 in the Supporting Information, while the side chain dihedral angle distributions, with their time evolution plots reported in the insets, are shown in Figure S7 in the Supporting Information. Similar to the Ala-Glu peptide case, ϕ distribution steeply falls from a maximum in the range [−180°,−150°] and vanishes at values beyond −120°, whereas ψ distribution is narrower than the Ala-Glu corresponding one and has a maximum in the range [75°,90°]. As a consequence backbone atoms of the Ala-Lys peptide are more constrained than the Ala-Glu ones. With the exception of χ_1, which has a more limited range of variation, side chain torsionals explore different angular domains, thus once again supporting the fact that side chains are much more flexible.

Time evolutions of the Ala-Lys atom surface distances are displayed in Figure 16, and the corresponding statistical data are reported in Table 2. As in the Ala-Glu dipeptide simulation C-terminal oxygens preserve their spatial arrangement, oscillating around a mean position located at a distance of ∼1.99 Å from the surface and of ∼2.03 Å from Ti sites, with σ equal to 0.05 Å.

The O_{CO} and H_{NH} surface distances fluctuate similarly, that is in a range having the same amplitude but around different mean values (6.57 Å for O_{CO} and 3.86 Å for H_{NH}). Larger fluctuations are observed for N-terminus distances that cover the range between 5.7 and 7.6 Å with σ = 0.32 Å.

The flexibility and conformation of the Lys side chain are highly variable and together with its spatial extent allow the NH_3^+ group to stretch toward the surface at the hydrogen-bonding distance. Such a behavior is apparent during the first

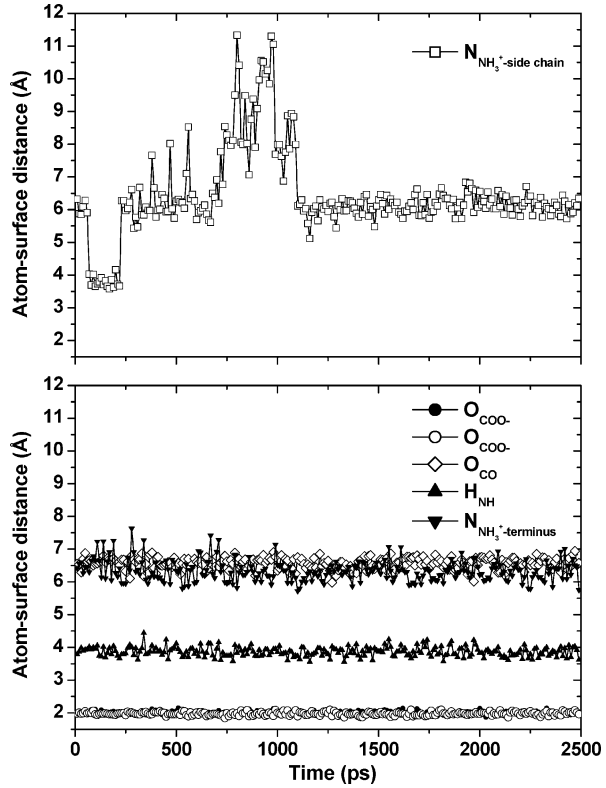

Figure 16. Evolution of the dipeptide Ala-Lys atom−surface distances during the molecular dynamics simulation time.

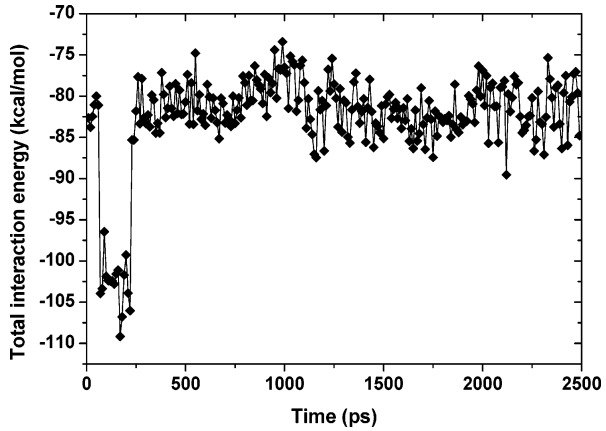

Figure 17. Evolution of the dipeptide Ala-Lys−surface interaction energy during the molecular dynamics simulation time.

250 ps of the trajectory where the amount of space between the $N_{NH_3^+}$ atom and the surface adopt values around 3.8 Å (Figure S8 in the Supporting Information). After this short time interval, the NH_3^+ group, in the subsequent simulation time, is shifted to longer distances and reaches, sometimes, the bulk region of the solvent.

The conformational changes of the Lys side chains and, above all, its nearness to the surface are reflected in the trend of the total interaction energy of this peptide with the TiO_2 layer (Figure 17). Indeed, the enhanced favorable interaction contemporaneous with the decrease in the $N_{NH_3^+}$ surface separation can be attributed to the addition of attractive contributions, mainly consisting of electrostatic terms coming from hydrogen-bonding interactions of the NH_3^+ moiety with the water molecules adsorbed onto the TiO_2 layer. During the rest of the simulation time an almost regular fluctuation of the Ala-Lys−surface interaction energy is observed.

Throughout 2.5 ns Lys and Glu side chains undergo major fluctuations, interacting favorably with water molecules and surface atoms. The additional flexibility of the N-terminal regions enables the side chains to switch between conformations extending into the bulk solvent and conformations in which the side chains forms hydrogen bonds with the interfacial adsorbed water molecules.

5. Conclusions

By comparison with ab initio calculations, Figure 8, we have shown that MD simulations of reasonable duration (2.5 ns) allow us to capture the essence of the peptide−TiO_2 surface interactions in solution at least on a short time scale. An amino acid (Ala) and two derived molecules (Ala-Ace and Ala-Nme), together with two dipeptides (Ala-Glu and Ala-Lys) "extracted" from the oligopeptide EAK16-II, adsorbed on the TiO_2 (110) rutile surface, have been studied for a number of possible adsorption geometries. Such adsorbates are quite stable and undergo relatively limited hinge-bending motions. Once bonded to the surface the peptides have a reasonable propensity to remain there, with the C-terminal polar group providing an anchor to the surface. Although it is clear from the analysis presented above that the conformational dynamics of the peptide side chains were not fully sampled, it is apparent that substantial changes only involve side chain dihedral angles and occur more frequently in the Ala-Glu dipeptide compared to the other dipeptide sequence. The trajectory for backbone ϕ and ψ angles has not revealed considerable fluctuations, which, however, seem to be slightly more marked for Ala-Glu than for Ala-Lys, although it is difficult to decide whether this difference is statistically significant. The average total number of water molecules hydrogen-bonded to the dipeptide hydrophilic groups is 13 in the case of the Ala-Lys sequence and 15 in the other model. These waters constitute a portion of a well-defined first solvation shell coordinated with the carboxyl, carbonyl, amide, and amine groups.

The high water activity prevents a strong peptide−surface interaction, but the adsorbed water layer plays an intermediary role, forming hydrogen-bond interactions with the hydrophilic groups of the peptide molecules.

The present paper can be considered a first positive report on the possibility of using atomistic molecular dynamics simulations, possibly complemented by ab initio calculations for limited portions of the system, to obtain information on the molecular structure and dynamics of peptides interacting with a TiO_2 surface in water solution. Investigations, by the same computational approach, on the adsorption on TiO_2 of larger peptides and in particular the ionic self-complementary oligopeptide EAK16-II, which is the final goal of our study, have been undertaken.

Acknowledgment. The authors thank Giovanni Polzonetti for bringing to their attention the interesting problem of the interaction of oligopeptides with TiO_2 surfaces.

Supporting Information Available: Van der Waals force field parameters in DL_POLY FIELD file format, radial distribution functions of surface atoms with water. evolution of the Ala-Nme−surface interaction energy during the molecular dynamics simulation time, evolution of the dipeptide Ala-Glu−surface interaction energy during the molecular dynamics simulation time, distribution of dipeptide Ala-Glu ϕ and ψ dihedral angles with their time evolution, distribution of dipeptide Ala-Glu χ_1 and χ_2 dihedral angles with their time

evolution, distribution of dipeptide Ala-Lys ϕ and ψ dihedral angles with their time evolution, distribution of dipeptide Ala-Lys χ_1, χ_2, χ_3, and χ_4 dihedral angles with their time evolution, and a simulation snapshot showing a representative structure of the Ala-Lys + (110) TiO_2 rutile layer + water complex having more favorable interaction energy values. This material is available free of charge via the Internet at http://pubs.acs.org.

References and Notes

(1) Zhang, S.; Holmes, T. C.; Lockshin, C.; Rich, A. *Proc. Natl. Acad. Sci. U.S.A.* **1993**, *90*, 3334−3338.

(2) Zhang, S.; Holmes, T. C.; Dipersio, C. M.; Hynes, R. O.; Su, X.; Rich, A. *Biomaterials* **1995**, *16*, 1385−1393.

(3) Holmes, T. C.; deLacalle, S.; Su, X.; Liu, G.; Rich, A.; Zhang, S. *Proc. Natl. Acad. Sci. U.S.A.* **2000**, *97*, 6728−6733.

(4) Zhang, S.; Altman, M. *React. Funct. Polym.* **1999**, *41*, 91−102.

(5) Nowak, A. P.; Breedvelt, V.; Pakstis, L.; Ozbas, B.; Pine, D. J.; Pochan, D.; Deming, T. J. *Nature* **2002**, *417*, 424−428.

(6) Zhang, S. *Biotechnol. Adv.* **2002**, *20*, 321−339.

(7) Hartgerink, D. J.; Beniash, E.; Stupp, S. I. *Science* **2001**, *294*, 1684−1687.

(8) Vanthey, S.; Santos, S.; Gong, H.; Watson, N.; Zhang, S. *Proc. Natl. Acad. Sci. U.S.A.* **2002**, *99*, 5355−5360.

(9) Whaley, S. R.; English, D. S.; Hu, E. L.; Barbara, P. F.; Belcher, A. M. *Nature* **2000**, *405*, 665−668.

(10) Lee, S. W.; Mao, C.; Flynn, C. E.; Belcher, A. M. *Science* **2002**, *296*, 892−895.

(11) Fung, S. Y.; Keyes, C.; Duhamel, J.; Chen, P. *Biophys. J.* **2003**, *85*, 537−548.

(12) Hong, Y.; Legge, R. L.; Zhang, S.; Chen, P. *Biomacromolecules* **2003**, *4*, 1433−1442.

(13) Altman, M.; Lee, P.; Rich, A.; Zhang, S. *Protein Sci.* **2000**, *9*, 1095−1105.

(14) Zhang, S.; Lockshin, C.; Cook, R.; Rich, A. *Biopolymers* **1994**, *34*, 663−672.

(15) Jun, S.; Hong, Y.; Imamura, H.; Ha, B. Y.; Bechhoefer, J.; Chen, P. *Biophys. J.* **2004**, *87*, 1249−1259.

(16) Diebold, U. *Surf. Sci. Rep.* **2003**, *48*, 53−229.

(17) Holmes, T. C. *Trends Biotechnol.* **2002**, *20*, 16−21.

(18) Schachner, M. *Nature* **2002**, *405*, 747−748.

(19) Kisiday, J.; Jin, M.; Kurz, B.; Hung, H.; Semino, C.; Zhang, S.; Grodzinsky, A. J. *Proc. Natl. Acad. Sci. U.S.A.* **2002**, *99*, 9996−10001.

(20) Zhang, Z.; Fenter, P.; Cheng, L.; Sturchio, N. C.; Bedzyk, M. J.; Predota, M; Bandura, A.; Kubicki, J. D.; Lvov, S. N.; Cummings, P. T.; Chialvo, A. A.; Ridley, M. K.; Benezeth, P.; Anovitz, L.; Palmer, D. A.; Machesky, M. L.; Wesolowski, D. J. *Langmuir* **2004**, *20*, 4954−4969.

(21) Predota, M.; Bandura, A. V.; Cummings, P. T.; Kubicki, J. D.; Wesolowski, D. J.; Chialvo, A. A.; Machesky, M. L. *J. Phys. Chem. B* **2004**, *108*, 12049−12060.

(22) *Cerius2 Modeling Environment*, version 4.0; Accelrys, Inc.: San Diego CA, 1999.

(23) Borodin, O.; Smith, G. D.; Bandyopadhyaya, R.; Byutner, O. *Macromolecules* **2003**, *36*, 7873−7883.

(24) Bandura, A. V.; Kubicki, J. *J. Phys. Chem. B* **2003**, *107*, 11072−11081.

(25) Cornell, W. D.; Cieplak, P.; Bayly, C. I.; Gould, I. R.; Merz, K. M. J.; Ferguson, D. M.; Spellmeyer, D. C.; Fox, T.; Caldwell, J. W.; Kollman, P. A. *J. Am. Chem. Soc.* **1995**, *117*, 5179−5197.

(26) Jorgensen, W. L. *J. Am. Chem. Soc.* **1981**, *103*, 335−350.

(27) Frisch, M. J.; Trucks, G. W.; Schlegel, H. B.; Scuseria, G. E.; Robb, M. A.; Cheeseman, J. R.; Montgomery, J. A., Jr.; Vreven, T.; Kudin, K. N.; Burant, J. C.; Millam, J. M.; Iyengar, S. S.; Tomasi, J.; Barone, V.; Mennucci, B.; Cossi, M.; Scalmani, G.; Rega, N.; Petersson, G. A.; Nakatsuji, H.; Hada, M.; Ehara, M.; Toyota, K.; Fukuda, R.; Hasegawa, J.; Ishida, M.; Nakajima, T.; Honda, Y.; Kitao, O.; Nakai, H.; Klene, M.; Li, X.; Knox, J. E.; Hratchian, H. P.; Cross, J. B.; Bakken, V.; Adamo, C.; Jaramillo, J.; Gomperts, R.; Stratmann, R. E.; Yazyev, O.; Austin, A. J.; Cammi, R.; Pomelli, C.; Ochterski, J. W.; Ayala, P. Y.; Morokuma, K.; Voth, G. A.; Salvador, P.; Dannenberg, J. J.; Zakrzewski, V. G.; Dapprich, S.; Daniels, A. D.; Strain, M. C.; Farkas, O.; Malick, D. K.; Rabuck, A. D.; Raghavachari, K.; Foresman, J. B.; Ortiz, J. V.; Cui, Q.; Baboul, A. G.; Clifford, S.; Cioslowski, J.; Stefanov, B. B.; Liu, G.; Liashenko, A.; Piskorz, P.; Komaromi, I.; Martin, R. L.; Fox, D. J.; Keith, T.; Al-Laham, M. A.; Peng, C. Y.; Nanayakkara, A.; Challacombe, M.; Gill, P. M. W.; Johnson, B.; Chen, W.; Wong, M. W.; Gonzalez, C.; Pople, J. A. *Gaussian 03*, revision A.1; Gaussian, Inc.: Wallingford, CT, 2004.

(28) Simon, S.; Duran, M.; Dannenberg, J. J. *J. Chem. Phys.* **1996**, *105*, 11024−11031.

(29) Boys, S. F.; Bernardi, F. *Mol. Phys.* **1970**, *19*, 553−566.

(30) Schmidt, M. *Arch. Orthop. Trauma Surg.* **2001**, *121*, 403−410.

(31) Bandura, V.; Sykes, D. J.; Shapovalov, V.; Truong, T. N.; Kubicki, J. D.; Evarestov, R. A. *J. Phys. Chem. B* **2004**, *108*, 7844−7853.

(32) Barnard, A. S.; Zapol, P.; Curtiss, L. A. *Surf. Sci.* **2005**, *582*, 173−188.

(33) Smith, W.; Forester, T. R. *J. Mol. Graphics* **1996**, *14*, 136−141.

(34) Hoover, W. G. *Phys. Rev. A* **1985**, *31*, 1695−1697.

(35) Allen, M. P.; Tildesley, D. J. *Computer Simulation of Liquids*; Clarendon Press: Oxford, U. K., 1989.

(36) Ryckaert, J. P.; Ciccotti, G.; Berendsen, H. J. C. *J. Comput. Phys.* **1977**, *23*, 327−341.

(37) Vittadini, A.; Selloni, A.; Rotzinger, F. P.; Grätzel, P. *J. Phys. Chem. B* **2000**, *104*, 1300−1306.

(38) Rego, L. G. C.; Batista, V. S. *J. Am. Chem. Soc.* **2003**, *125*, 7989−7997.

(39) Foster, A. S.; Gal, A. Y.; Nieminen, R. M.; Shluger, A. L. *J. Phys. Chem. B* **2005**, *109*, 4554−4560.

(40) Iucci, G.; Carravetta, V.; Altamura, P.; Russo, M. V.; Paolucci, G.; Goldoni, A.; Polzonetti, G. *Chem. Phys.* **2004**, *302*, 43−52.

(41) Roddick-Lanzilotta, A. D.; Connor, P. A.; McQuillan, A. J. *Langmuir* **1998**, *14*, 6479−6484.

(42) Persson, P.; Lunell, S.; Bruhwiler, P. A.; Schnadt, J.; Sodergren, S.; O'Shea, J. N.; Karis, O.; Siegbahn, H.; Bassler, N. M. M.; Patthey, L. *J. Chem. Phys.* **2000**, *112*, 3945−3948.

(43) Odelius, M.; Persson, P.; Lunell, S. *Surf. Sci.* **2003**, *529*, 47−58.

(44) Hammer, B.; Hansen, L. B.; Norskov, K. J. *Phys. Rev. B* **1999**, *59*, 7413−7421.

(45) Greeley, J.; Norskov, K. J.; Mavrikakis, M. *Annu. Rev. Phys. Chem.* **2002**, *53*, 319−348.

(46) Epling, W. S.; Peden, C. H. F.; Henderson, M. A.; Diebold, U. *Surf. Sci.* **1998**, *412*, 333−343.

(47) Diebold, U.; Madey, T. E. *J. Vac. Sci. Technol., A* **1992**, *10*, 2327−2335.

(48) Diebold, U.; Madey, T. E. *Springer Ser. Surf. Sci.* **1993**, *31*, 284−288.

(49) Román, E. L.; de Segovia, J. L. *Surf. Sci.* **1991**, *251/252*, 742−746.

(50) Román, E. L.; de Segovia, J. L.; Kurtz, R. L.; Madey, T. E. *Surf. Sci.* **1992**, *273*, 40−46.

(51) Markovits, A.; Ahdjoudj, J.; Minot, C. *Surf. Sci.* **1996**, *365*, 649−661.

(52) Paschek, D.; Geiger, A. *AIP Conf. Proc.* **1995**, *330*, 349−355.